4090 *Macromolecules* **2009**, *42*, 4090–4098
DOI: 10.1021/ma9004988

Macromolecules
ARTICLE

Solvent-Induced Association and Micellization of Rod−Coil Diblock Copolymer

Weiran Lin, Jie Zhang, Xinhua Wan,* Dehai Liang,* and Qifeng Zhou

Beijing National Laboratory for Molecular Sciences, Key Laboratory of Polymer Chemistry & Physics of Ministry of Education, College of Chemistry & Molecular Engineering, Peking University, Beijing 100871, P. R. China

Received November 24, 2008; Revised Manuscript Received April 9, 2009

ABSTRACT: The solvent-induced association and micellization processes of amphiphilic rod−coil diblock copolymers, poly(ethylene oxide)-*b*-poly{(+)-2,5-bis[4'-((*S*)-2-methylbutoxy)phenyl]styrene} (PEO_{104}-*b*-$PMBPS_n$, with *n* being 17, 30, 45, 53, and 106, respectively), were studied in situ by laser light scattering. In dioxane, a selective solvent for PMBPS block, the copolymer preserved the single-chain conformation. With the addition of water, a selective solvent for PEO block, the block copolymer underwent two difference processes: the association governed by PEO and the micellization governed by PMBPS. Because PMBPS would be dominant at elevated water content, three occurrences, the formation of associate, the formation of micelles, and the breakdown of associate, were observed in sequence with increasing water content. However, under the conditions where the rate of disassociation was much slower than that of micellization, the structure of the associate was "frozen" by the rod blocks, and mixed structures of associate and micelle were obtained. The associate formed at elevated water content was controlled by kinetics. Its formation was mainly determined by the PEO/PMBPS block ratio and the water addition rate.

Introduction

The self-assembly behaviors of amphiphilic block copolymers in aqueous solution have been well studied in the past few decades.[1−6] It is generally believed that three factors, that is, the core-chain stretching entropy, the core−corona interfacial energy, and the intercoronal chain repulsive interaction, govern the structures of the aggregates formed by coil−coil block copolymers.[4] With proper control over these three factors by tuning the external conditions (solvent property,[7,8] pH,[9] ion strength,[8,10] and temperature[9,11]), block copolymers are manipulated to form a wide range of morphologies, such as spheres, rods, vesicles, and large compound micelles (LCMs). Kinetic control of the aggregate morphologies by altering preparation methods has also received much attention from experimental and theoretical viewpoints.[12−18]

Besides the chemical composition, the conformation of the block, for example, rigid rod versus flexible coil, also shows profound effect on the self-assembly of the block copolymers. Rod−coil block copolymers consisting of both flexible and rigid segments were endowed with various functionalities through the rod blocks, and have attracted a lot of attention from biologists, chemists, and physicists.[5,19−23] Different types of rigid polymers have been employed as the rod blocks, such as conjugated polymers,[24−26] helical polymers,[27,28] liquid crystalline polymers,[29] and crystallizable polymers.[30,31] The conformational asymmetry between the rod and coil blocks, the preferred parallel orientation, and the slow mobility of rigid segment in such copolymers showed a remarkable influence on their self-assembly behaviors. In particular, Jenekhe and Chen revealed the specific single-layer structure of the vesicles from poly(phenylquinoline)-*b*-polystyrene diblock copolymers due to the enhanced shell stiffness and the surface tension from high in-plane order of rigid poly(phenylquinoline) block.[24,25] Disklike aggregates were reported for rod−coil block copolymer of poly(*n*-hexyl isocyanate)-*b*-poly(ethylene glycol) (PHIC-*b*-PEG).[32] In a series of amphiphilic block copolymers containing side-chain liquid-crystalline polymers as the hydrophobic core-forming segments, Li and coworkers found that a smectic ordering in the bulk was responsible for the nanofiber formation in water.[29]

In a theoretical study of diblock copolymers, it has been found that the increase in the stiffness of the insoluble block decreased the critical micelle concentration and increased the average micelle size.[33] Therefore, the rod block generally played a key role during the assembly of the block copolymer in selective solvent. In a previous study,[34] we demonstrated that the rod block, poly{(+)-2,5-bis[4'-((*S*)-2-methylbutoxy)phenyl]styrene} (PMBPS), dominated the micellization process of its copolymer with poly(ethylene oxide) (PEO). In pure dioxane, a selective solvent for PMBPS but a precipitant for PEO block, PEO_{104}-*b*-$PMBPS_{53}$ maintained its single chain conformation at concentrations up to 1.0×10^{-3} g/mL.[34] Novel structures or morphologies would be formed if the leading role of the block was switched during the assembly process. To prove this hypothesis, we studied the water-induced aggregation process of PEO-*b*-PMBPS in dioxane by using laser light scattering (LLS) and transmission electron microscopy (TEM) in this work. With the molecular weight of PEO being constant at 5000, the polymerization degree of the PMBPS block was varied from 17 to 106. Besides changing the block length, we also varied the water content as well as the water-addition rate to tune the role of the blocks and the kinetics of the polymer chains.

Experimental Section

Laser Light Scattering Measurement. Five PEO_{104}-*b*-$PMBPS_n$ block copolymers (Chart 1), with *n*, the degree of polymerization of PMBPS, being 17, 30, 45, 53, and 106, respectively, were synthesized and purified according to a

*Corresponding author. (D.L.) E-mail: dliang@pku.edu.cn. Tel: 10-86-62756170. (X.W.) E-mail: xhwan@pku.edu.cn. Tel: 10-86-62754187.

 Published on Web 05/06/2009

Chart 1. Chemical Structure of the Rod−Coil Diblock Copolymer PEO_{104}-*b*-$PMBPS_n$

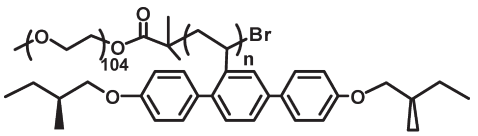

PEO_{104}-*b*-$PMBPS_n$

n = 17, 30, 45, 53,106

known procedure.[35,36] The polymer samples of known amount were dissolved in HPLC grade dioxane to obtain homogeneous solutions at least one night before the measurement. The final concentration was 1.0 mg/mL for all samples. For LLS measurement, about 2 mL of polymer solution was filtered directly into a dust-free cylindrical light-scattering cell through a 0.22 μm pore size Millex filter unit (Millipore, Billerica, MA). Deionized water (Milli-Q, resistance = 18.2 MΩ) filtered through a 0.22 μm pore size filter unit was added dropwise to the copolymer solution. By a general procedure, one drop of water (~1.0 wt % of the solution) was added at each interval, and the polymer solution was vortexed at 600 rpm for about 5 min. The sample solution was then allowed to sit at 25°C for at least 40 min before the measurement was carried out. Scattered light intensity was used to check the equilibrium.

A commercial LLS spectrometer (Brookhaven, Holtsville, NY) equipped with a BI-200SM goniometer and a BI-Turbo-Corr digital correlator was used to perform both static light scattering (SLS) and dynamic light scattering (DLS) over scattering angles ranging from 20 to 120°. A 100 mW, vertically polarized solid-state laser (GNI, Changchun, China) operating at 532 nm was used as the light source. In SLS, the angular dependence of the excess absolute time-averaged scattered intensity, also known as the Rayleigh ratio, $R_{vv}(\theta)$, was measured. From the angular dependence of $R_{vv}(\theta)$ in a single concentration, the apparent *z*-average root-mean-square radius of gyration, $R_{g,app}$, was obtained. In dynamic LLS, the intensity−intensity time correlation function $G^{(2)}(t)$ in the self-beating mode was measured. It is related to the normalized first-order electric field time correlation function $g^{(1)}(t)$. A Laplace inversion program, CONTIN, was applied to analyze $g^{(1)}(t)$ to obtain the hydrodynamic radius, $R_{h,app}$, and its distribution. The $R_{g,app}/R_{h,app}$ values at different water contents were calculated by a combination of the results from SLS and DLS.[37,38]

Transmission Electron Microscopy (TEM) Measurement. The morphologies of the aggregates were observed on a JEM-200CX TEM operating at an acceleration voltage of 120 kV. After LLS experiments, the solution in each stage was poured in a large amount of water to freeze the aggregate structures instantly.[4] The resulting colloidal solution was transferred to dialysis tubes (Huamei Bio-Engineering, molecular weight cutoff 14 000 Da) and dialyzed against deionized water for 3 days to remove organic solvent. Deionized water was changed three times a day. For the TEM experiment, a drop of the sample solution was mixed with a drop of 2% (w/v) aqueous solution of uranyl acetate. The mixture was deposited onto a carbon-coated copper EM grid for a few minutes. Excess solution was blotted away with a strip of filter paper, and the sample grid was dried in air.

Results and Discussion

PEO_{104}-*b*-$PMBPS_n$ in Dioxane. Because dioxane is a good solvent for PMBPS but a nonsolvent for PEO,[39] it was expected that PEO would induce PEO_{104}-*b*-$PMBPS_n$ to aggregate in dioxane.[32,40] However, no aggregate formation was evidenced from the LLS measurements. As indicated in Figure 1, the selected copolymers, PEO_{104}-*b*-$PMBPS_{17}$, PEO_{104}-*b*-$PMBPS_{45}$, and PEO_{104}-*b*-$PMBPS_{106}$ exhibited a monodistribution at 1.0 mg/mL. The average $R_{h,app}$ values were 2.2, 3.4, and 4.8 nm, respectively, which were close to the sizes of single polymer chains. Also, because of the small sizes of the polymer chains, the excess scattered intensity showed almost no angular dependence (inset in Figure 1). It has been documented that dioxane is a nonsolvent for PEO.[39] Our LLS experiment showed that PEO with $M_w \approx 5000$ displayed microphase separation in pure dioxane at 1.0 mg/mL (data not shown). The possible reason that PEO_{104}-*b*-$PMBPS_n$ failed to form micelle lies in the fact that the condensed PEO chains were not strong enough to form aggregates because the rigid, bulky PMBPS blocks take more than 60 wt % mass of the block copolymers.[41]

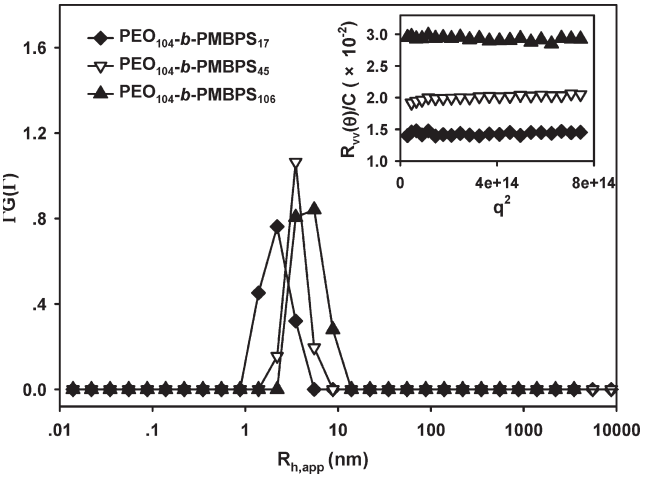

Figure 1. CONTIN analyses of the rod−coil block copolymers PEO_{104}-*b*-$PMBPS_n$ with *n* being 17, 45, and 106, respectively, in dioxane at 1.0 mg/mL at 30°. The inset shows the angular dependence of the excess scattered intensities.

PEO_{104}-*b*-$PMBPS_n$ with Longer PMBPS Length. Figure 2 shows the LLS results of PEO_{104}-*b*-$PMBPS_{106}$ in dioxane after the addition of a different amount of water. The micelles with PMBPS being the core and PEO being the corona were formed after the addition of 3.3 wt % water (Figure 2A). No single polymer chain was observed under such conditions. With further addition of water content to ~28 wt %, the size of the micelles remained almost constant at ~30 nm (Figure 2B). In brief, PEO_{104}-*b*-$PMBPS_{106}$ underwent a normal solvent-induced micellization process.

The aggregation process of PEO_{104}-*b*-$PMBPS_{53}$ is similar to that of PEO_{104}-*b*-$PMBPS_{106}$, except that an associate with $R_{h,app} \approx 100$ nm was observed at 4.8 wt % water content. As shown in Figure 3A, the associate coexisted with the single polymer chains in the system. However, with one more drop of water to increase the water content to 5.6 wt %, both the single chains and the associate disappeared. What formed in the system was the micelles with $R_{h,app} \approx 20$ nm (Figure 3B). With further addition of water, the aggregation behavior of PEO_{104}-*b*-$PMBPS_{53}$ followed a trend similar to that of PEO_{104}-*b*-$PMBPS_{106}$ (Figure 3C). Because of the smaller size of the micelles and the single chains, no apparent angular dependence of the excess scattered intensity was observed with increasing water content (Figure 3D), except at the point (4.8 wt %) when the associate was formed. As shown in the inset of Figure 3D, the excess scattered intensity at 30° was at least three times larger than that at 90° at 4.8 wt % water content, which was caused by the association of polymer chains.

PEO_{104}-*b*-$PMBPS_{45}$ in Dioxane/H_2O. As discussed above (Figure 3C), PEO_{104}-*b*-$PMBPS_{53}$ formed the associate in a

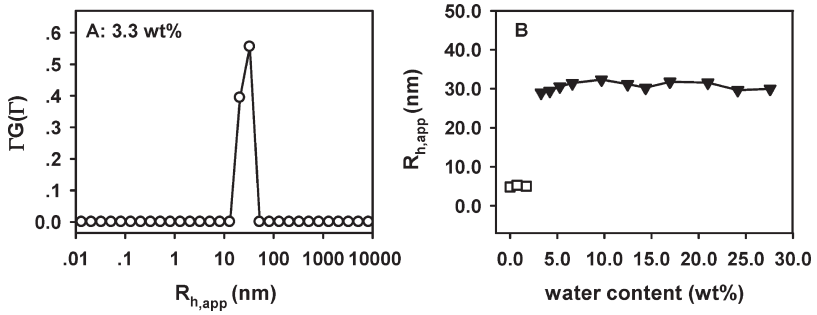

Figure 2. LLS results of PEO_{104}-*b*-$PMBPS_{106}$: (A) CONTIN analysis of the correlation function measured at 30°; (B) changes in $R_{h,app}$ after extrapolation to zero angle.

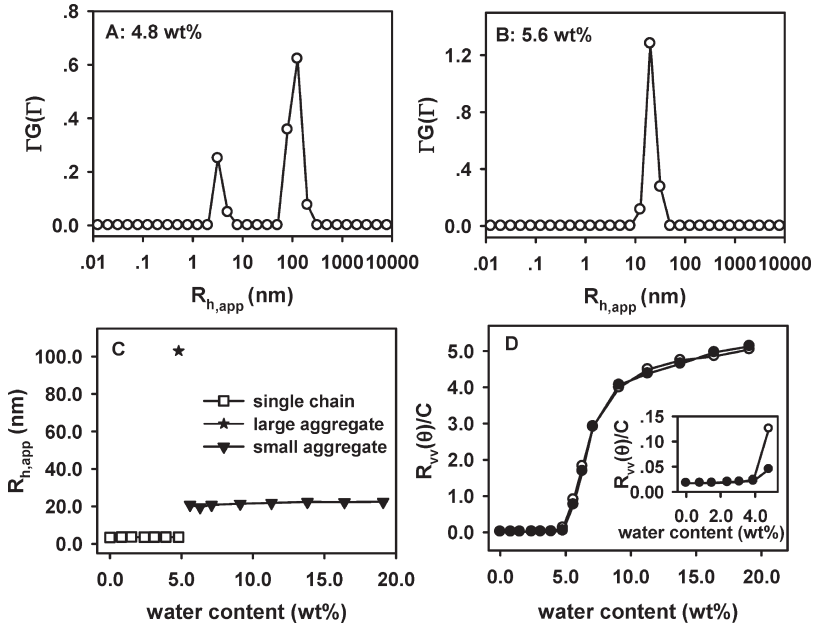

Figure 3. LLS results of PEO_{104}-*b*-$PMBPS_{53}$: (A,B) CONTIN analysis of the correlation functions measured at 30°; (C) changes in $R_{h,app}$ after extrapolation to zero angle; (D) changes in $R_{vv}(\theta)/C$ at 30° (−○−) and 90° (−●−). The inset shows the data at the water content before 5.0 wt %

very narrow water content range. However, the stability of the associate was significantly improved when the block copolymer with shorter PMBPS block was used. Figure 4 shows the DLS results of PEO_{104}-*b*-$PMBPS_{45}$ in dioxane after the addition of a different amount of water. The associate with $R_{h,app} \approx 80$ nm was first observed at 3.6 wt % water content (Figure 4A), less than that (4.8 wt %) for PEO_{104}-*b*-$PMBPS_{53}$, and it was stable even after the formation of the micelles, as shown in Figure 4B, where the single polymer chains disappeared and the micelles with $R_{h,app} \approx 15$ nm coexisted with the associates. With further increasing water content to 28.6 wt %, the associate survived and suffered only a slight decrease in area ratio (Figure 4C). This solution was quite stable, and no appreciable change was observed from the measurement of LLS after standing at room temperature for about a week.

Figure 4D shows the $R_{h,app}$ values after extrapolation to zero angle. The size of the associate increased very quickly at the very beginning. At 6.2 wt % water content when the micelles formed, its size was increased to 170 nm. After reaching its maximum value of 257 nm at 8.8 wt % water content, the $R_{h,app}$ value slowly declined to reach a constant value. As for the micelle, the $R_{h,app}$ gradually increased from 14.6 to 19.5 nm in the ~6.2−8.8 wt % water content range and then remained almost constant.

Figure 5 shows the changes in the excess scattered light intensity at 30 and 90° with increasing water content. The data were corrected by concentration for accuracy and for better comparisons. Without aggregation, the excess scattered intensity was almost invariable and showed no angular dependence. After the formation of the associate at 3.6 wt % water content, the excess scattered intensity clearly displayed three stages: (1) Below 6.2 wt % water content, where the micelle was not formed, the excess scattered intensity slightly increased and showed a strong angular dependence (Figure 5A); a typical pronounced downward curve at lower scattering angle due to the existence of the associate was observed (Figure 5C).[38] (2) From 6.2 to 8.8 wt % water content, the excess scattered intensity sharply increased, owing to the appearance of the micelles and the increases in size of both the micelle and the associate (Figure 5B). (3) Above 8.8 wt % water content, the increases in the excess scattered intensity slowed down. Because of the coexistence of the micelle and the associate, the excess scattered intensity also went downward at lower scattering angles (Figure 5D).

Because the associate always coexisted with either the single polymer chains or the micelles, it was difficult to determine its $R_{g,app}$ values. In the systems with bimodal distributions, Sato and coworkers[42] demonstrated that the static structure factors ($S(q)$) of the fast mode and the slow mode were able to be calculated separately by the combination of the SLS and DLS data. The radius of gyration was then obtained from the $S(q)$. The detailed procedure can be

found in refs 42 and 43. By using the scattering data at 30, 45, 60, 75, and 90°, we calculated the $S(q)$ of the slow mode and, consequently, the $R_{g,app}$ of the associate. As shown in Figure 6, $R_{g,app}$ of the associate followed a trend similar to that of $R_{h,app}$. The conformation of the associate could be inferred from the R_g/R_h ratio. It was well established in literature that the R_g/R_h ratios were 0.775 and 1.5 for solid sphere and random coil, respectively.[37] The inset in Figure 6 shows the $R_{g,app}/R_{h,app}$ values of the large aggregates formed by PEO_{104}-*b*-$PMBPS_{45}$ at different water contents. The monotonic decrease from 1.6 at the beginning to 0.78 at 8.8 wt % water content indicated that the associate underwent a morphological change from loose coil structure to a more condensed packing. With further increasing water content to 28.6 wt %, $R_{g,app}/R_{h,app}$ maintained a constant value of around 0.85, indicating that the structure of the associate was kept stable.

PEO_{104}-*b*-$PMBPS_n$ with Shorter PMBPS. With further decreasing PMBPS block length, the associate became unstable. Figure 7 shows the size distribution of PEO_{104}-*b*-$PMBPS_{30}$ at different water contents. The associate was formed after the addition of a very small amount of water (2.2 wt %) (Figure 7A). The size and ratio of the associate increased with the water content. At 9.2 wt % water content, micelle with $R_{h,app}$ of 12.0 nm was formed, and it coexisted with single polymer chains and the associate (Figure 7B). With further increasing water content, the single polymer chains quickly disappeared, and the area ratio of the associate decreased as well. At 12.2 wt % water content, the micelle was the dominant component in the system, and the amount of the associate was negligible (Figure 7C). Figure 7D displays the $R_{h,app}$ changes of the single chains, the associates, and the micelles at different water contents. Clearly, the associate formed by PEO_{104}-*b*-$PMBPS_{30}$ exhibited a trend

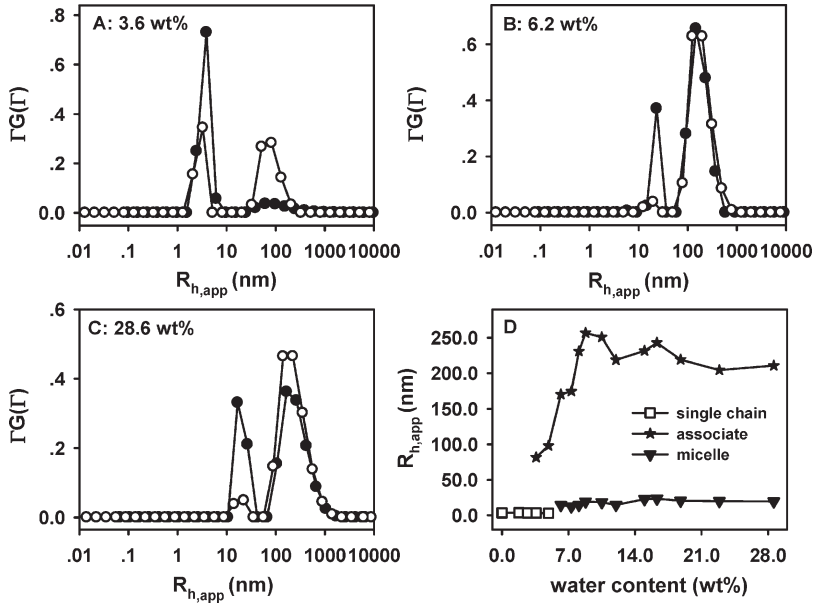

Figure 4. DLS results of PEO_{104}-*b*-$PMBPS_{45}$: (A−C) CONTIN analysis of the correlation functions measured at 30° (−○−) and 90° (−●−); (D) changes in $R_{h,app}$ after the extrapolation to zero angle.

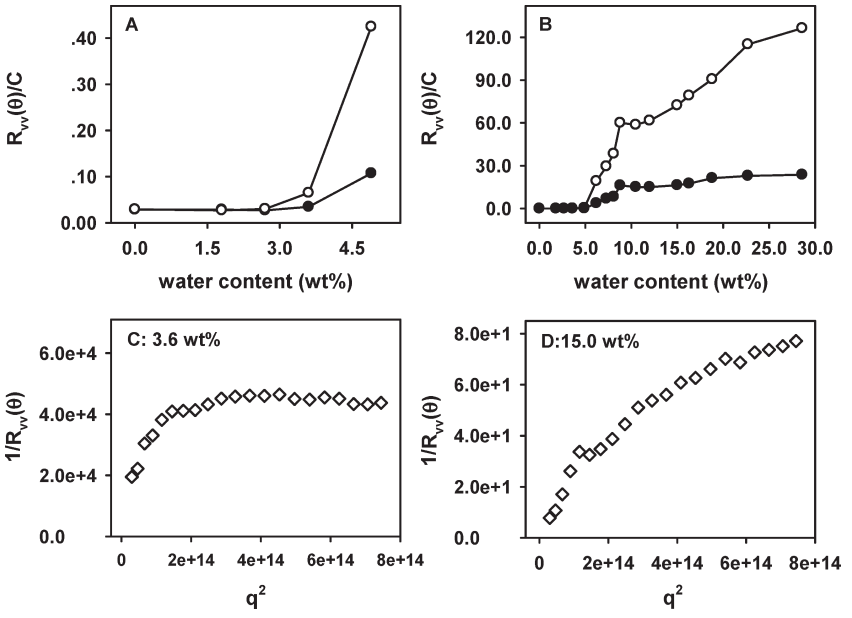

Figure 5. SLS results of PEO_{104}-*b*-$PMBPS_{45}$: (A,B) changes in $R_{vv}(\theta)/C$ at 30° (−○−) and 90° (−●−) with increasing water content; (C) angular dependence of $1/R_{vv}(\theta)$ at 3.6 wt % water content and (D) at 15.0 wt % water content.

similar to that formed by PEO_{104}-*b*-$PMBPS_{45}$ (Figure 4D), except that the associate formed by PEO_{104}-*b*-$PMBPS_{30}$ sharply decreased in size and quickly disappeared. The aggregation process of PEO_{104}-*b*-$PMBPS_{17}$ was similar to that of PEO_{104}-*b*-$PMBPS_{30}$. (See Figure S1 in the Supporting Information.) The major difference was that the associate was formed after the addition of an even smaller amount of water (1.9 wt %) but disappeared after the addition of a larger amount of water (17.2 wt %).

Transmission Electron Microscopy Results. To demonstrate the existence of the associate and to show its difference from the micelles, we conducted TEM experiments on selected samples after their morphologies were frozen by the addition of a large amount of water.[4] Figure 8A shows the TEM images of PEO_{104}-*b*-$PMBPS_{45}$ at 28.6 wt % water content. Consistent with LLS results (Figure 4C), large spherical structures with a diameter of more than 100 nm coexisted with the micelles whose diameter was about 27 nm. The large structure exhibited a broader size distribution than micelles. Efforts have also been paid to freeze the associate formed before the appearance of micelles (~6 wt %). Unfortunately, only micellar structures were observed, suggesting that the loose aggregates were in a fast equilibrium with the single chains and could not be frozen simply by adding large amounts of water. It also indicated that the conformation of the associate in equilibrium with the single chains (Figure 4A) was different from that of the associated in equilibrium with the micelles (Figure 4B), which agreed with the results in Figure 6.

Figure 8B shows the TEM images of PEO_{104}-*b*-$PMBPS_{30}$ at 9.8 wt % water content, where the micelles have already been formed. Similar large spherical structure was visualized (Figure 8B). However, no such structures were observed by TEM at elevated water content (Figure 8C), which is consistent with the LLS results (Figure 7D).

Mechanism of Association. Table 1 summarizes the association and micellization results of the five block copolymer as well as their physicochemical data. The water-induced micellization process of PEO_{104}-*b*-$PMBPS_n$ is rational and understandable. Water is a poor solvent for PMBPS; for example, at 0.7 mg/mL, PMBPS with 40 repeating units started to aggregate at ~ 5 wt % water content. (See Figure S2 of the Supporting Information.) It was believed that the core-forming block played a key role in determining the critical micelle points and the micelle size.[44] Therefore, the water content at which the micelles started to form was decreased with increasing PMBPS block length, whereas the $R_{h,app}$ of the micelles showed the opposite trend (Table 1). However, the water content at which the associate started to form increased with the PMBPS block length, and no associate was formed when the PMBPS length increased to

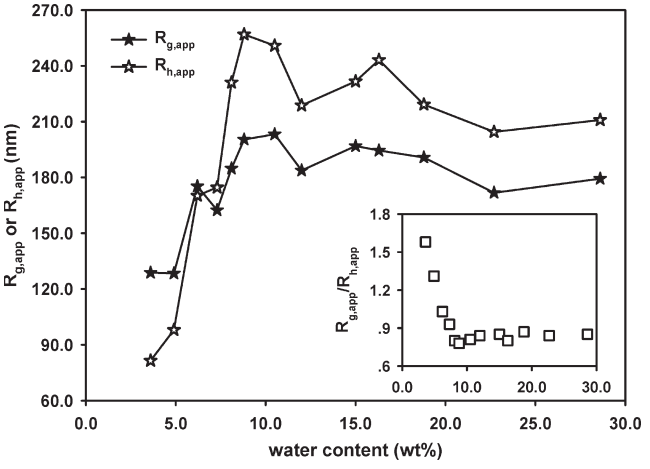

Figure 6. $R_{g,app}$ and $R_{h,app}$ of the associate formed by PEO_{104}-*b*-$PMBPS_{45}$ with increasing water content. The line is used to guide the eyes. The inset shows the changes in the $R_{g,app}/R_{h,app}$ ratio.

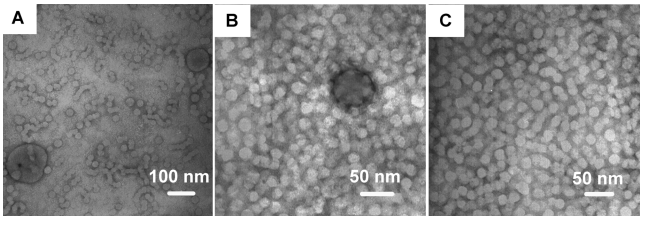

Figure 8. Typical TEM images of (A) PEO_{104}-*b*-$PMBPS_{45}$ at 28.6 wt % water content, (B) PEO_{104}-*b*-$PMBPS_{30}$ at 9.8 wt % water content, and (C) PEO_{104}-*b*-$PMBPS_{30}$ at 26.9 wt % water content.

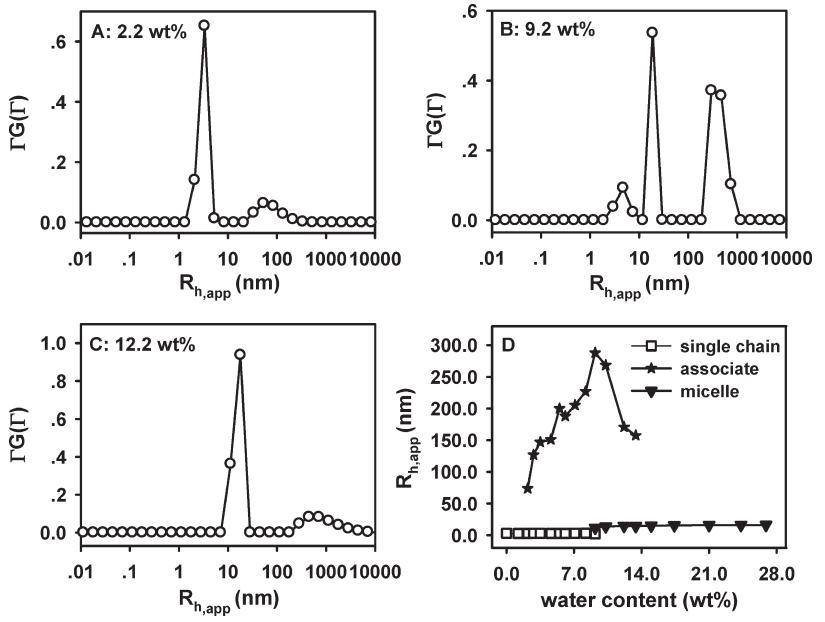

Figure 7. DLS results of PEO_{104}-*b*-$PMBPS_{30}$: (A–C) CONTIN analysis of the correlation functions measured at 30°; (D) changes in $R_{h,app}$ after the extrapolation to zero angle.

Table 1. Macromolecular Properties of PEO_{104}-*b*-$PMBPS_n$ and Their Self-Assembly Behaviors in Dioxane/Water

				water content (wt %)			
copolymers	M_n (10^4 Da)[a]	PDI[a]	weight fraction of PMBPS	associate form	micelle form	associate disappear	micelle size $R_{h,app}$ (nm)
PEO_{104}-*b*-$PMBPS_{17}$	1.19	1.09	0.61	1.9	12.5	17.2	14.2
PEO_{104}-*b*-$PMBPS_{30}$	1.74	1.11	0.74	2.2	9.2	13.4	16.1
PEO_{104}-*b*-$PMBPS_{45}$	2.39	1.13	0.81	3.6	6.2	28.6[b]	19.7
PEO_{104}-*b*-$PMBPS_{53}$	2.71	1.12	0.83	4.8	5.6	5.6	22.3
PEO_{104}-*b*-$PMBPS_{106}$	4.98	1.19	0.91	N/A	3.3	N/A	30.0

[a] Results from GPC. [b] Maximum value tested.

106. In other words, the PMBPS block did not favor the formation of the associate. Therefore, the driving force for the associate can only come from the PEO block. Because of the specific interaction between PEO and water,[45−48] the absorption of water molecule by PEO in dioxane, a poor solvent, was likely to occur. The PEO with the surrounding water acted together as a hydrophilic block and led to the association of PEO_{104}-*b*-$PMBPS_n$. At lower water content when PMBPS blocks stayed as individual chains, the associate was in equilibrium with the single polymer chains, and the associate contained many loose domains rich of water and PEO. The association of block copolymers became stronger with increasing water content. At a certain point, whose value was dependent on the block ratio, PMBPS block started to aggregate, leading to the formation of micelles with PMBPS being the core and PEO being the corona. In the meantime, the chain density of the associate also increased because of the same reason. Clearly, both the micelle and the associate were formed by the same polymer chains, but they were different in structure and morphology. Therefore, a competition between the associate and the micelle started to exist. Block ratio and water content were two major factors to determine the ultimate structures. Because the weight fraction of PMBPS block was larger than that of PEO (even in PEO_{104}-*b*-$PMBPS_{17}$) and the attractive interaction between PMBPS blocks became stronger with increasing water content, the micelle would eventually dominant in the system. Therefore, the breakdown of the associate was mainly determined by PMBPS block. It was reasonable that the water content at which the associate started to disappear decreased with increasing the PMBPS block (Table 1). However, the data in Figure 4 and Table 1 indicated that PEO_{104}-*b*-$PMBPS_{45}$ was an exception to this rule: the associate it formed did not disappear, even at 28.6 wt % water content.

The above discussion was solely based on thermodynamics. Kinetics may play a key role under certain circumstances. The breakdown of the associate and the formation of the micelle were two separated processes, both of which possessed a characteristic lifetime (or residence time of single polymer chains). The time scale was closely related to the block length and the stability of the structure (associate or micelle). If the rate of disassociation was faster than or comparable to that of the micellization, then the micelle, which was thermodynamically stable, would be the ultimate structure. The block copolymers with shorter PMBPS block (the micellization rate was slow) or longer PMBPS block (the associate was not stable and quickly breakdown) belong to this case. However, if the micellization rate was much faster than the disassociation rate, then the structure of the associate could be "frozen" by the PMBPS blocks. A mixed structure of associate and micelle was obtained, which could be the case of PEO_{104}-*b*-$PMBPS_{45}$.

To testify our hypothesis, we conducted the water-induced aggregation of PEO_{104}-*b*-$PMBPS_{45}$ in dioxane by adding water at a faster rate. We added ~3 wt % water at each interval, and the aging time was decreased to 10 min. Under such circumstance, PEO may not have enough time to form stable associate before the micellization starts. Casually formed associate should break down at a fast rate. As shown in Figure 9, the associate formed by PEO_{104}-*b*-$PMBPS_{45}$ was first observed at 30° at 5.2 wt % water content (Figure 9A). The addition of water one more time to 8.1 wt % surpassed the critical micelle point (6.2 wt %) of PEO_{104}-*b*-$PMBPS_{45}$, and the micelle was quickly formed. Different from that at slow water addition rate, no associate was observed once the micelle was formed (Figure 9B). With further addition of water to 27.7 wt %, the micelle with $R_{h,app} \approx 20$ nm existed in the system (Figure 9C,D). The results in Figure 9 demonstrated that the associate that coexisted with the micelle was controlled by kinetics. Note that Figure 9 shows results similar to those of Figure 3. It was reasonable because the breakdown of the associate formed by PEO_{104}-*b*-$PMBPS_{45}$ at faster water-addition rate was due to the unstability of the associate, which followed a similar rule as that of the block copolymer with longer PMBPS block.

The data in Figure 6 indicated that the conformation and property of the associate could be different at the water content before and after the micelle formation. To prove this point further, we conducted two experiments by using PEO_{104}-*b*-$PMBPS_{45}$: first, water was slowly added to the system to 4.5 and 6.6 wt %, separately; then, a faster water-addition rate (~ 3 wt % per 10 min) was employed to introduce a large amount of water. Figure 10 compares the DLS results of the two experiments. As shown in Figure 10A, the associate was formed at 4.5 wt % water content, and it was in equilibrium with the single polymer chains. Compared with the data in Figure 4, the ratio of the associate significantly decreased after the quick addition of water content to 20.7 wt % (Figure 10B). However, if the associate was in equilibrium with the micelle (Figure 10A′), then the quick addition of water showed less effect on the ratio of the associate, even at higher water content, 28.7 wt % (Figure 10B′). Because the associate was controlled by kinetics, the results in Figure 10 indicated that the lifetime of the associate in equilibrium with single polymer chains was shorter than that in equilibrium with micelles. In other words, the residence time of polymer chains in the associate was significantly increased after the formation of micelles. The addition of a larger amount of water after the formation of micelle could not break down the associate.

Figure 11 schematically shows the water-induced association and micellization process of PEO_{104}-*b*-$PMBPS_n$ in dioxane. Within a certain block ratio, the associate, governed by the coil block PEO, was formed at a certain water content (slow addition of water), and it was in equilibrium with the single polymer chains (panel B). Further addition of water above the critical micelle point switched the leading force to PMBPS block; micelles with PMBPS being the core and PEO being the coronal were formed, and it was

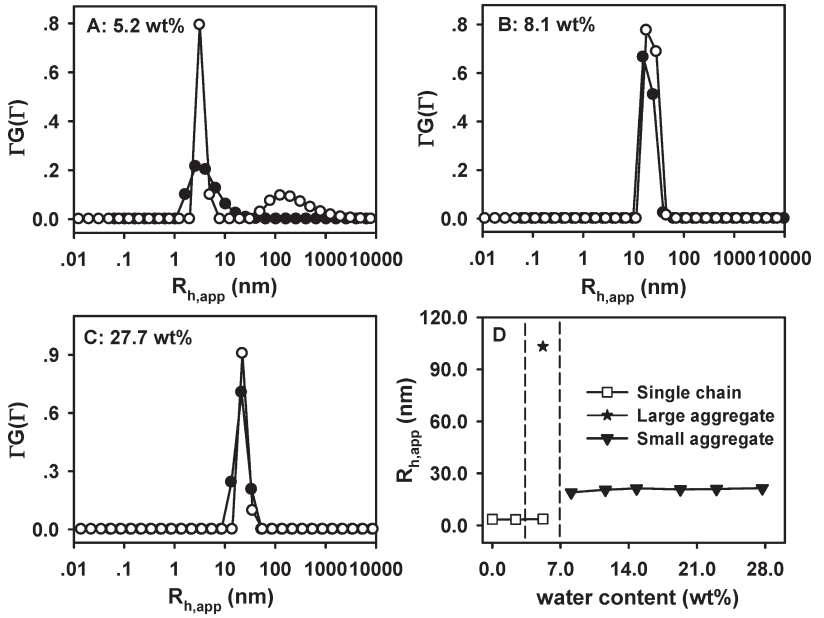

Figure 9. DLS results of PEO_{104}-*b*-$PMBPS_{45}$ at fast water-addition rate: (A−C) CONTIN analysis of the correlation functions measured at 30° (−○−) and 90° (−●−); (D) changes in $R_{h,app}$ after extrapolation to zero angle.

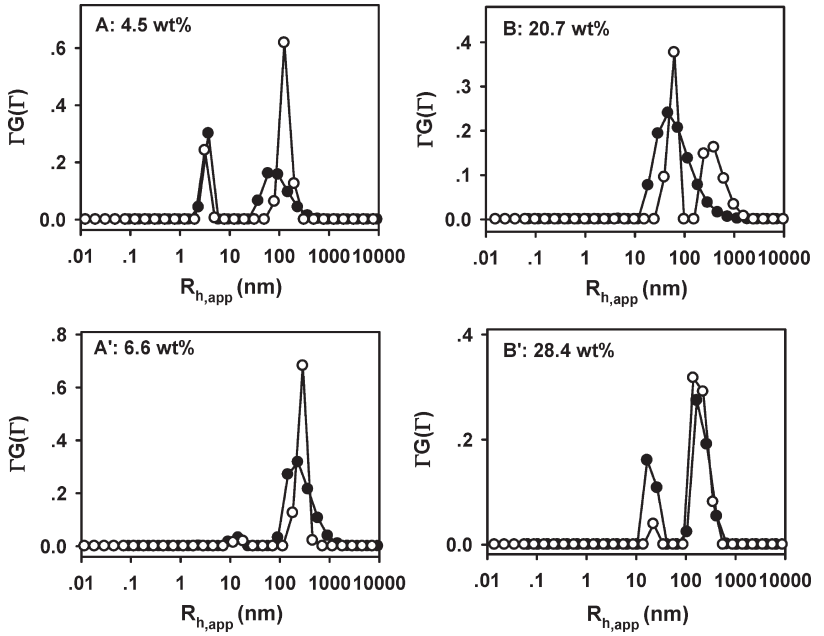

Figure 10. Size distribution of PEO_{104}-*b*-$PMBPS_{45}$ at different water content: (A) slowly adding water to 4.5 wt %; (B) followed by quickly adding water to 20.7 wt %; (C) slowly adding water to 6.6 wt %; (D) followed by quickly adding water to 28.4 wt %.

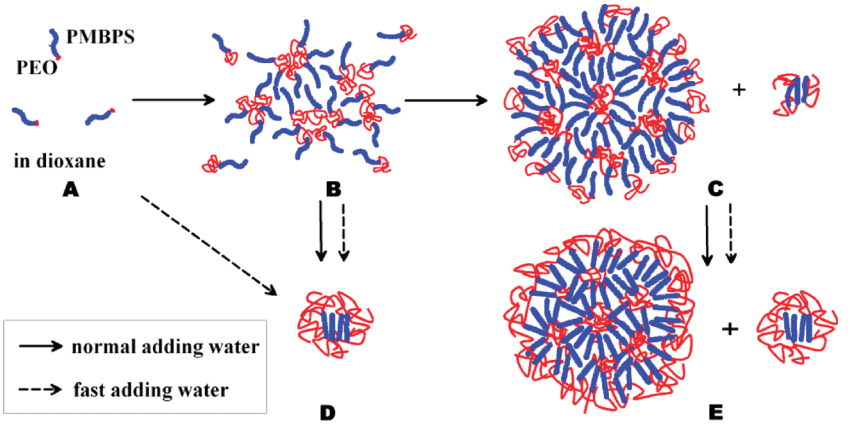

Figure 11. Schematic showing the water induced association and micellization processes of PEO_{104}-*b*-$PMBPS_n$ in dioxane.

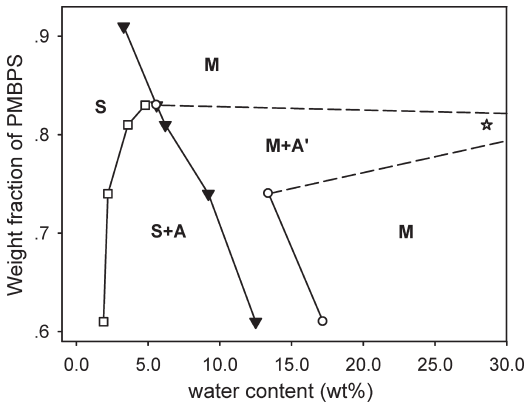

Figure 12. Phase diagram of PEO-*b*-PMBPS in mixed solvent of dioxane and water. The curves were drawn on the basis of the data in Table 1: (S) single polymer chain, (A) loose associate, (M) micelle, (A′) condensed associate. The dashed lines represent the estimated boundary.

thermodynamically stable (panel D). Under certain conditions, the associate formed by the block copolymer with proper block ratio was kinetically stable (panel C); the addition of a large amount of water resulted in the mixed structure of associate and micelle (panel E).

A phase diagram was drawn on the basis of the data in Table 1 and the above discussion on the mechanism. Depending on the water content and the block ratio, four distinct zones were formed by PEO-*b*-PMBPS in mixed solvent of dioxane and water (Figure 12). Besides the commonly observed single polymer chains (S) and the micelles (M), the loose associate (A) and the condensed associate (A′), coexisting with S and M, respectively, were formed in sequence with water content. Their borderline was the micellization curve. The condensed associate, A′, controlled by kinetics, was closely related to the water-addition rate. As indicated by the dashed lines, the M + A′ phase did not have a sharp boundary with the M phase.

The assembly of PEO-*b*-PMBPS in mixed solvent involved two basic structures (associate and micelles) and one type of interaction (excluded volume interaction). It could serve as a simple model to reveal some basic principles about the kinetic-controlled structures: (1) The aggregation process involves at least two different structures; each dominates in a certain stage or time period. The forces maintaining the structures may or may not be the same. (2) Upon turning over, the former aggregate should be strong enough to hold, at least partially, its structure before of the latter aggregate matures. (3) To build a strong energy barrier to prevent the relaxation of the former aggregate, the driving force for the latter aggregate should be reinforced, or it should be in a "frozen" state. These principles could be applied to the kinetic-controlled structures reported in literature. In general, the intermolecular electrostatic interaction is stronger than the excluded volume interaction and also exhibits a much longer working range; it is easy to "trap" the kinetic-controlled structures.[16−18,49] The chain block, whose glass-transition point was far below room temperature, such as polystyrene, was also a good choice to "freeze" the structures.[16,18]

Conclusions

Block copolymers have the capacity to form diverse assembled structures in the solvent selective for one of the blocks. The variety of structures showed many practical or potential applications in the field of solubilizers, dispersion agents, nanomaterials, drug delivery vehicles, and so on. In this work, we have demonstrated that the rod−coil diblock copolymer, PEO_{104}-*b*-$PMBPS_n$, was able to form either micelles or the mixed structures of micelles with certain associate. The associate was kinetically stable. Even though the two structures are formed by the same polymer, their size and property are quite different; for example, the associate contains many hydrophilic domains. Therefore, the mixed structures provide extra functions and may have some potential applications.

Acknowledgment. This work is financially supported by the National Natural Science Foundation of China (grants 20504001 and 20674001) and the National Distinguished Young Scholar Fund (grant 20325415).

Supporting Information Available: Dynamic light scattering results on homopolymer $PMBPS_{40}$ and block copolymer of PEO_{104}-*b*-$PMBPS_{17}$ at different water contents. This material is available free of charge via the Internet at http://pubs.acs.org.

References and Notes

(1) Lehn, J. M. *Supramolecular Chemistry: Concepts and Perspectives*; VCH: Weinheim, Germany, **1995**.
(2) Hadjichristidis, N.; Pispas, S.; Floudas, G. *Block Copolymers: Synthetic Strategies, Physical Properties, and Applications*; John Wiley & Sons, Inc.: Hoboken, N.J., **2003**.
(3) Halperin, A. *Macromolecules* **1987**, *20*, 2943.
(4) Cameron, N. S.; Corbierre, M. K.; Eisenberg, A. *Can. J. Chem.* **1999**, *77*, 1311.
(5) Lee, M.; Cho, B. K.; Zin, W. C. *Chem. Rev.* **2001**, *101*, 3869.
(6) Vriezema, D. M.; ComellasAragones, M.; Elemans, J. A. A. W.; Cornelissen, J. J. L. M.; Rowan, A. E.; Nolte, R. J. M. *Chem. Rev.* **2005**, *105*, 1445.
(7) Yu, Y. S.; Eisenberg, A. *J. Am. Chem. Soc.* **1997**, *119*, 8383.
(8) Choucair, A.; Lavigueur, C.; Eisenberg, A. *Langmuir* **2004**, *20*, 3894.
(9) Liu, F.; Eisenberg, A. *J. Am. Chem. Soc.* **2003**, *125*, 15059.
(10) Yuan, G.; Wang, X.; Han, C. C.; Wu, C. *Macromolecules* **2006**, *39*, 6207.
(11) Bhargava, P.; Tu, Y.; Zheng, J. X.; Xiong, H.; Quirk, R. P.; Cheng, S. Z. D. *J. Am. Chem. Soc.* **2007**, *129*, 1113.
(12) Tian, M.; Qin, A.; Ramireddy, C.; Webber, S. E.; Munk, P.; Tuzar, Z.; Prochazka, K. *Langmuir* **1993**, *9*, 1741.
(13) Lund, R.; Willner, L.; Richter, D.; Dormidontova, E. E. *Macromolecules* **2006**, *39*, 4566.
(14) Colombani, O.; Ruppel, M.; Burkhardt, M.; Drechsler, M.; Schumacher, M.; Gradzielski, M.; Schweins, R.; Müller, A. H. E. *Macromolecules* **2007**, *40*, 4351.
(15) Ji, S. C.; Ding, J. D. *Langmuir* **2006**, *22*, 553.
(16) Zhang, L. F.; Eisenberg, A. *Macromolecules* **1999**, *32*, 2239.
(17) Cui, H.; Chen, Z.; Zhong, S.; Wooley, K. L.; Pochan, D. J. *Science* **2007**, *317*, 647.
(18) Pochan, D. J.; Chen, Z.; Cui, H.; Hales, K.; Qi, K.; Wooley, K. L. *Science* **2004**, *306*, 94.
(19) Kim, B. S.; Hong, D. J.; Bae, J.; Lee, M. *J. Am. Chem. Soc.* **2005**, *127*, 16333.
(20) Tung, Y. C.; Wu, W. C.; Chen, W. C. *Macromol. Rapid Commun.* **2006**, *27*, 1838.
(21) Lin, S. L.; Numasawa, N.; Nose, T.; Lin, J. P. *Macromolecules* **2007**, *40*, 1684.
(22) Duan, H. W.; Kuang, M.; Wang, J.; Chen, D. Y.; Jiang, M. *J. Phys. Chem. B* **2004**, *108*, 550.
(23) Tu, Y.; Wan, X.; Zhang, D.; Zhou, Q.; Wu, C. *J. Am. Chem. Soc.* **2000**, *122*, 10201.
(24) Jenekhe, S. A.; Chen, X. L. *Science* **1998**, *279*, 1903.
(25) Jenekhe, S. A.; Chen, X. L. *Science* **1999**, *283*, 372.
(26) Stupp, S. I.; Lebonheur, V.; Walker, K.; Li, L. S.; Huggins, K. E.; Keser, M.; Amstutz, A. *Science* **1997**, *276*, 384.
(27) Rodriguez-Hernandez, J.; Lecommandoux, S. *J. Am. Chem. Soc.* **2005**, *127*, 2026.
(28) Cornelissen, J. J. L. M.; Fischer, M.; Nolte, R. J. M. *Science* **1998**, *280*, 1427.
(29) Piñol, R.; Jia, L.; Gubellini, F.; Lévy, D.; Albouy, P. A.; Keller, P.; Cao, A.; Li, M. H. *Macromolecules* **2007**, *40*, 5625.

(30) Raez, J.; Manners, I.; Winnik, M. A. *J. Am. Chem. Soc.* **2002**, *124*, 10381.
(31) Wang, X.; Guerin, G.; Wang, H.; Wang, Y.; Manners, I; Winnik, M. A. *Science* **2007**, *317*, 644.
(32) Wu, J.; Pearce, E. M.; Kwei, T. K.; Lefebvre, A. A.; Balsara, N. P. *Macromolecules* **2002**, *35*, 1791.
(33) Adriani, P.; Wang, Y.; Mattice, W. L. *J. Chem. Phys.* **1994**, *100*, 7718.
(34) Zhang, J.; Lin, W.; Liu, A.; Yu, Z.; Wan, X.; Liang, D.; Zhou, Q. *Langmuir* **2008**, *24*, 3780.
(35) Zhang, J.; Yu, Z. N.; Wan, X. H.; Chen, X. F.; Zhou, Q. F. *Macromol. Rapid Commun.* **2005**, *26*, 1241.
(36) Yu, Z. N.; Wan, X. H.; Zhang, H. L.; Chen, X. F.; Zhou, Q. F. *Chem. Commun.* **2003**, *8*, 974.
(37) Burchard, W. *Adv. Polym. Sci.* **1983**, *48*, 1.
(38) *Light Scattering from Polymer Solution*; Huglin, M. B., Ed.; Academic Press: New York, **1972**; p 132.
(39) Brandrup, J; Immergut, E. H. *Polymer Handbook*, 3rd ed.; Wiley-Interscience: New York, **1989**, Vol. *VII*, p. 519.
(40) Burkhardt, M.; Martinez-Castro, N.; Tea, S.; Drechsler, M.; Babin, I.; Grishagin, I.; Schweins, R.; Pergushov, D. V.; Gradzielski, M.; Zezin, A. B.; Müller, A. H. E. *Langmuir* **2007**, *23*, 12864.
(41) Liu, A.; Zhi, J.; Cui, J.; Wan, X.; Zhou, Q. *Macromolecules* **2007**, *40*, 8233.
(42) Kanao, M.; Matsuda, Y.; Sato, T. *Macromolecules* **2003**, *36*, 2093.
(43) Aono, H.; Tatsumi, D.; Matsumoto, T. *Biomacromolecules* **2006**, *7*, 1311.
(44) Zhang, L.; Eisenberg, A. *Polym. Adv. Tech.* **1998**, *9*, 677.
(45) Polik, W. F.; Burchard, W. *Macromolecules* **1983**, *16*, 978.
(46) Hammouda, B.; Ho, D.; Kline, S. *Macromolecules* **2002**, *35*, 8578.
(47) Kjellander, R.; Florin, E. *J. Chem. Soc., Faraday Trans. 1* **1981**, *77*, 2053.
(48) Bronstein, L. M.; Chernyshov, D. M.; Timofeeva, G. I.; Dubrovina, L. V.; Valetsky, P. M. *Langmuir* **1999**, *15*, 6195.
(49) Kötz, J.; Kosmella, S.; Beitz, T. *Prog. Polym. Sci.* **2001**, *26*, 1199.